Received 16 February 2019
Revised 16 February 2019
Accepted 18 March 2019

Analysis of kinematic dexterity and stiffness performance based on Spring's wire-driven 4-SPS/U rigid–flexible parallel trunk joint mechanism

Yitao Pan
School of Mechanical, Electrical and Information Engineering, Shandong University at Weihai, Weihai, China
Yuan Chen
Shandong University at Weihai, Weihai, China, and
Lin Li
School of Mechanical, Electrical and Information Engineering, Shandong University at Weihai, Weihai, China

Abstract

Purpose – The purpose of this paper is to propose a two-degrees-of-freedom wire-driven 4SPS/U rigid–flexible parallel trunk joint mechanism based on spring, in order to improve the robot's athletic ability, load capacity and rigidity, and to ensure the coordination of multi-modal motion.

Design/methodology/approach – First, based on the rotation transformation matrix and closed-loop constraint equation of the parallel trunk joint mechanism, the mathematical model of its inverse position solution is constructed. Then, the Jacobian matrix of velocity and acceleration is derived by time derivative method. On this basis, the stiffness matrix of the parallel trunk joint mechanism is derived on the basis of the principle of virtual work and combined with the deformation effect of the rope driving pair and the spring elastic restraint pair. Then, the eigenvalue distribution of the stiffness matrix and the global stiffness performance index are used as the stiffness evaluation index of the mechanism. In addition, the performance index of athletic dexterity is analyzed. Finally, the distribution map of kinematic dexterity and stiffness is drawn in the workspace by numerical simulation, and the influence of the introduced spring on the stiffness distribution of the parallel trunk joint mechanism is compared and analyzed. It is concluded that the stiffness in the specific direction of the parallel trunk joint mechanism can be improved, and the stiffness distribution can be improved by adjusting the spring elastic structure parameters of the rope-driven branch chain.

Findings – Studies have shown that the wire-driven 4SPS/U rigid–flexible parallel trunk joint mechanism based on spring has a great kinematic dexterity, load-carrying capacity and stiffness performance.

Research limitations/implications – The soft-mixed structure is not mature, and there are few new materials for the soft-mixed mixture; the rope and the rigid structure are driven together with a large amount of friction and hindrance factors, etc.

Practical implications – It ensures that the multi-motion mode hexapod mobile robot can meet the requirement of sufficient different stiffness for different motion postures through the parallel trunk joint mechanism, and it ensures that the multi-motion mode hexapod mobile robot in multi-motion mode can meet the performance requirement of global stiffness change at different pose points of different motion postures through the parallel trunk joint mechanism.

Social implications – The trunk structure is a very critical mechanism for animals. Animals in the movement to achieve smooth climbing, overturning and other different postures, such as centipede, starfish, giant salamander and other multi-legged animals, not only rely on the unique leg mechanism, but also must have a unique trunk

International Journal of Structural Integrity
Vol. 10 No. 6, 2019
pp. 850-867
Emerald Publishing Limited
1757-9864
DOI 10.1108/IJSI-02-2019-0010

joint mechanism. Based on the cooperation of these two mechanisms, the animal can achieve a stable, flexible and flexible variety of motion characteristics. Therefore, the trunk joint mechanism has an important significance for the coordinated movement of the whole body of the multi-sport mode mobile robot (Huang Hu-lin, 2016).

Originality/value – In this paper, based on the idea of combining rigid parallel mechanism with wire-driven mechanism, a trunk mechanism is designed, which is composed of four spring-based wire-driven 4SPS/U rigid–flexible parallel trunk joint mechanism in series. Its spring-based wire-driven 4SPS/U rigid–flexible parallel trunk joint mechanism can make the multi-motion mode mobile robot have better load capacity, mobility and stiffness performance (Qi-zhi *et al.*, 2018; Cong-hao *et al.*, 2018), thus improving the environmental adaptability and reliability of the multi-motion mode mobile robot.

Keywords Stiffness matrix, Stiffness analysis, Dexterity analysis, Trunk joint mechanism, Wire driven

Paper type Research paper

1. Introduction

The trunk structure is a very critical mechanism for animals. Animals in the movement to achieve smooth climbing, overturning and other different postures, such as centipede, starfish, giant salamander and other multi-legged animals, not only rely on the unique leg mechanism, but also must have a unique trunk joint mechanism. Based on the cooperation of these two mechanisms, the animal can achieve a stable, flexible and flexible variety of motion characteristics. Therefore, the trunk joint mechanism has an important significance for the coordinated movement of the whole body of the multi-sport mode mobile robot (Huang Hu-lin, 2016).

The WABIAN-2R robot developed by Waseda University in Japan has a trunk driven in series and consists of two parts: hip and waist. Its trunk design with more degrees of freedom enables the robot to have better motion performance, such as the realization of more human-like gait movement. It rotates the pelvis, so that the legs are fully extended as the robot steps forward, unlike other robots that need to bend the knees to maintain balance. In addition, it can also achieve the complex movement of outward skimming legs and keep balance while standing on the cushion layer. But its waist mechanism also has the structure complexity, the mass overweight and so on (Kanehiro *et al.*, 2003; Ogura *et al.*, 2006). The I Struct ape-like space exploration robot jointly developed by the German artificial intelligence research center and the university of Bremen (Metta *et al.*, 2008) has a 6-dof parallel mechanism for its trunk, which makes the robot have good bearing capacity, improves the rigidity of the robot, reduces error accumulation and improves the motion accuracy. Because of the light mass and low inertia of moving parts, the dynamic performance of the system is improved. However, this kind of mechanism also has the problem of small range of motion, which limits the robot to carry out large and flexible motion. The i Cub robot (Beira *et al.*, 2006) developed by the European Association of Innovation Universities, in which the two degrees of freedom of pitch and deflection are based on a wire rope-driven differential mechanism; the degree of freedom of the roll is achieved by servo motor drive. This kind of flexible wire drive makes the humanoid robot flexible at the waist, but this kind of drive also has the problem of small driving force/torque, which makes it difficult to maintain sufficient stiffness under the circumstance of large driving load. To sum up, the early trunk joint mechanism has advantages and disadvantages: the tandem mechanism is complex and the quality is too heavy; the rigid parallel mechanism has less range of activities and low flexibility; and low bearing capacity and low stiffness of wire-driven mechanism.

In the face of complex ground environment and diverse operational requirements, higher requirements are put forward for the environmental adaptability and the whole body coordination movement ability of multi-motion mode mobile robot. Therefore, the trunk joint mechanism not only can achieve multi-attitude adjustment, but it also needs large stiffness and dexterity (Jian-feng *et al.*, 2016) to maintain the posture accuracy (Portman *et al.*, 2012) of the wooden end and large bearing capacity. In this paper, based on the idea of combining rigid parallel mechanism with wire-driven mechanism, a trunk mechanism is designed, which is composed of four spring-based wire-driven 4SPS/U rigid–flexible parallel trunk joint mechanism in series. Its spring-based wire-driven 4SPS/U rigid–flexible parallel trunk joint

mechanism can make the multi-motion mode mobile robot have better load capacity, mobility and stiffness performance (Qi-zhi *et al.*, 2018; Cong-hao *et al.*, 2018), thus improving the environmental adaptability and reliability of the multi-motion mode mobile robot.

First, the coordinates of the spring-based wire-driven 4SPS/U rigid–flexible parallel trunk joint mechanism are established, and the inverse kinematic position solution model of the mechanism is established by using the closed vector method, and the Jacobian matrix of velocity and acceleration is obtained. Then, combining the influence of wire of the driving part (Hai-wei *et al.*, 2013; Run-tian, 2016) and the spring elastic deformation of the restraint part (Zhe-dong *et al.*, 2018; Fan, 2014), the performance indexes of the kinematic dexterity and mechanism stiffness are established. Finally, the distribution map of the kinematic performance index of the configuration mechanism in the workspace is drawn by numerical simulation, and the kinematic dexterity and stiffness of the mechanism are analyzed.

2. Innovative design of the wire-driven 4-SPS/U rigid–flexible parallel trunk joint mechanism based on spring

Similar to Figure 1, the multi-movement mode mobile robot consists of a head structure, a leg mechanism, a trunk mechanism and a propeller propulsion structure. The leg mechanism is made up of forward, middle and rear leg devices. The trunk mechanism is the critical shifting part of the multi-movement mode mobile robot, which is composed of four spring-based rope-driven 4-SPS/U rigid–flexible parallel body joint mechanisms. As shown by Figure 1(a), the multi-movement mode mobile robot can perform different posture adjustments through the trunk joint mechanism, thereby enabling the variable direction bending trajectory crawling between the front, middle, and rear legs. As shown by Figure 1(b), after the six legs are contracted, the vector propulsion between the head structure and the propeller propulsion structure at the tail can be realized through the posture diversity adjustment of the trunk joint mechanism. As shown by Figure 1(c), when climbing obstacles, such as stairs and ditches, the robot can adjust the bending changes of different parts of the body through the trunk joint mechanism to adjust the position of the center of gravity between the middle, front and middle

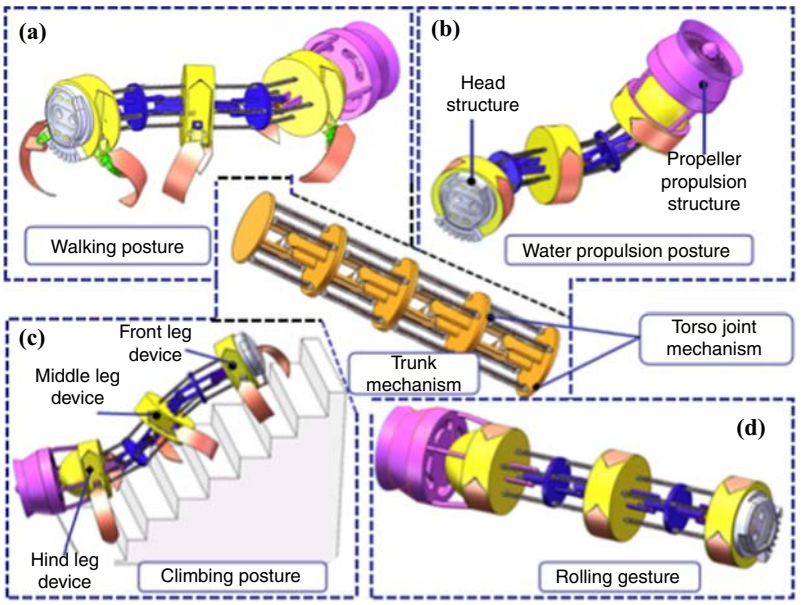

Figure 1.
Structure composition and motion posture of mobile robot in multi-motion mode

hind legs, so as to improve the climbing ability. As shown by Figure 1(d), the multi-movement mode mobile robot contracts the six legs at the smooth and gentle slopes, and adjusts the bending and twisting between different parts of the torso through the trunk joint mechanism to achieve a snake-like crawling. It is also possible to perform an overall rolling motion.

As shown by Figure 2(a), the wire-driven 4-SPS/U rigid–flexible parallel trunk joint mechanism is composed of the dynamic platform and the static platform, as well as the constraint branch chain and the drive branch chain connecting the dynamic platform and the static platform. As shown in the middle of Figure 2(a), the drive branch chain includes four wire-driven SPS rigid–flexible branches with the same structure. As shown in the upper right and lower right part of Figure 2(a), the upper and lower spherical hinges are, respectively, assembled in the spherical hinges of the dynamic and static platforms, and the spring seat is set for the upper spherical hinge and the spring seat for the lower spherical hinge. As shown in the upper left part Figure 2(a), embedding the spring in the spring base between the upper and lower spherical hingers can improve the rigidity. As shown by the picture of the lower right of Figure 2(a), piercing hole is set at the bottom of each spherical hinge seat on the static platform and also at the center of the lower spherical hinge. Then one end of the rope goes through the hole in the spherical hinge seat of the static platform, through the spring between the upper and lower spherical hinge springs, and is finally fixed on the spring seat of the upper ball joint, and the other end is fixed on the wire fixing frame of the stranding wheel at the bottom of the static platform. Thus, a spring-based wire-driven SPS rigid–flexible branching chain is assembled. As shown by the picture of lower left in Figure 2(a), the constraint branch chain assembles the shaft end of the Hooke hinge in the same direction between the two sides of the dynamic and static platform through the sliding bearing, forming an intermediate passive constraint branched chain U. A corresponding drive motor for each drive branch chain is set at the bottom of the static platform, and each drive motor is provided with a stranded wheel. By driving the motor to drive the winch wheel, the driving rope on the driving branch chain is wound around, so that the length of the rope is shortened. When the winch wheel releases the driving rope line on its driving branch chain, the rope line is elongated under the spring elastic action line. Thereby, the telescopic movement of the rope drive branches realized (Qing-huan *et al.*, 2017; Trevisani *et al.*, 2006; Von Zitzewitz *et al.*, 2013; Jun, 2016; Dong-tao *et al.*, 2013), and the rotational torque of the motor output is converted into linear thrust and tension.

As shown by Figure 2(b), the spherical pair connected to the static platform is set as the first kinematic pair, the shifting pair is set as the second kinematic pair, and the spherical pair connected to the dynamic platform is set to be the third kinematic pair. O_A-$X_AY_AZ_A$ and O_B-$X_BY_BZ_B$ are the static coordinate system and moving coordinate system at the circle center of the static platform and moving platform, respectively, O_A point is at the circle center of the static platform with radius r, X_A axis is along with A_3A_1, Y_A axis is along with A_4A_2, Z_A axis accordance with right-hand rule. O_B is at the circle center of the mobile platform with radius r, X_B axis is along with B_3B_1, Y_B axis is along with B_4B_2 and Z_B axis is in accordance with the right hand rule.

3. The kinematics modeling of the wire-driven 4-SPS/U rigid–flexible parallel trunk joint mechanism

3.1 Inverse solution model of position

As shown in Figure 3, coordinate systems O_A-$X_AY_AZ_A$, O_C-$X_CY_CZ_C$ and O_B-$X_BY_BZ_B$ are, respectively, established at the center of the static platform, the moving platform, and the hook hinge. The spherical hinge points at both ends of the four driving SPS branch chains are located at the points A_1, A_2, A_3 and A_4 on the static platform, and at the points B_1, B_2, B_3 and B_4 on the moving platform, and are evenly and symmetrically distributed. The distance between the static platform and the moving platform spherical hinge point to the center of

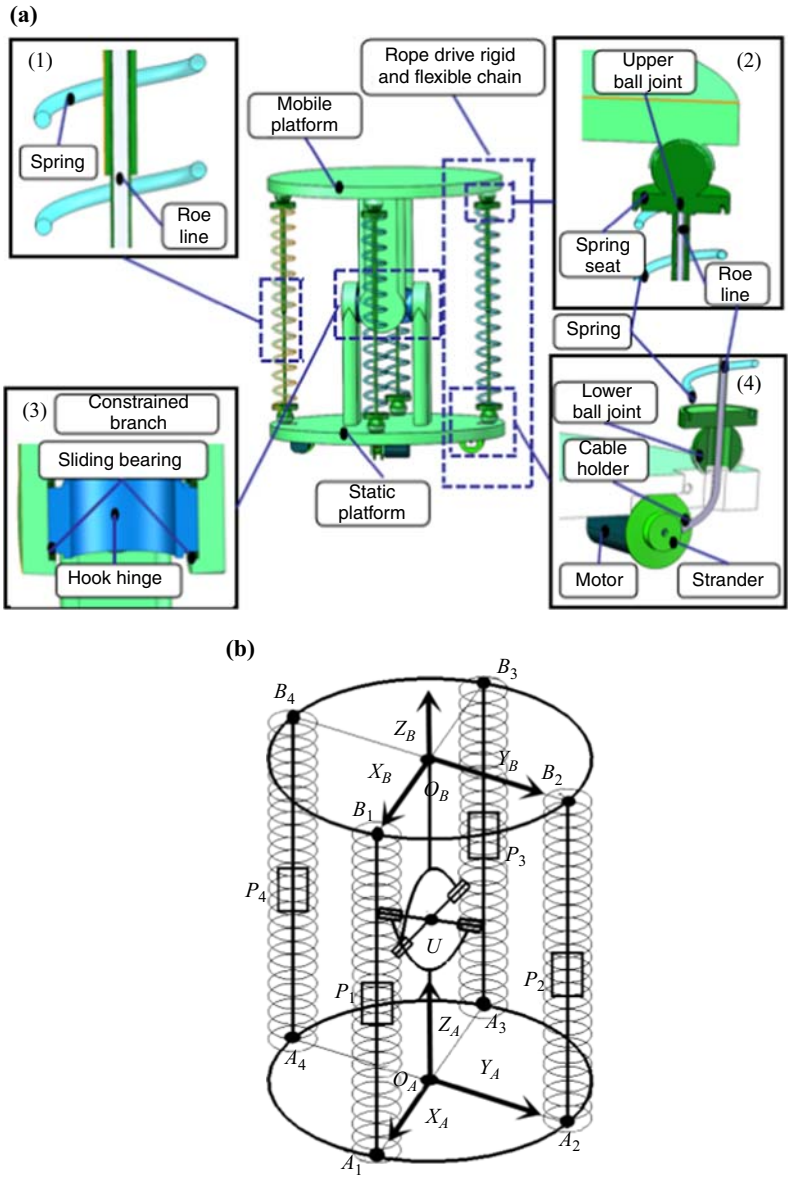

Figure 2.
Wire-driven 4-SPS/U rigid–flexible parallel trunk joint mechanism

Notes: (a) The three-dimension graph of wire-driven 4-SPS/U trunk joint mechanism; (b) simplified drawing of wire-driven 4-SPS/U Trunk Joint Mechanism

the circle is r. The intermediate constraint branch U is located between the static platform and the moving platform, and the distance from the center of the Hook hinge to the center of the upper and lower platforms is l.

As shown by Figure 3, the coordinate system O_C-$X_CY_CZ_C$ at the center of the Hooke hinge rotates around Y_C axis at the angle of θ_2, and the dynamic coordinate system O_B-

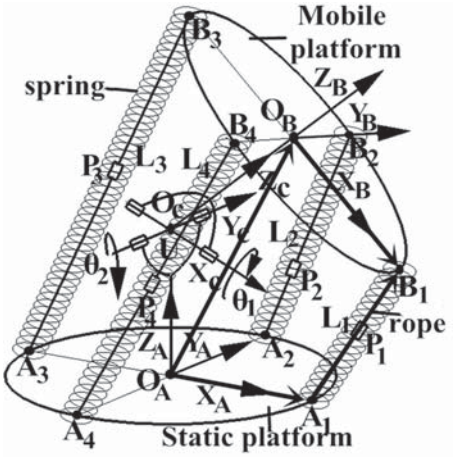

Figure 3.
Simplified drawing of wire-driven 4-SPS/U Trunk Joint Mechanism

$X_BY_BZ_B$ rotates around X_C axis at the angle of θ_1. Then, the homogeneous transformation matrix (Craig, 2009) of the moving coordinate system O_B-$X_BY_BZ_B$ relative to the static system O_A-$X_AY_AZ_A$ can be obtained as follows:

$$
\begin{aligned}
{}^{A}_{B}T &= \mathrm{Trans}(0,0,l)\mathrm{Rot}(y,\theta_2)\mathrm{Rot}(x,\theta_1)\mathrm{Trans}(0,0,l) \\
&= \begin{bmatrix} C\theta_2 & S\theta_2 S\theta_1 & S\theta_2 C\theta_1 & lS\theta_2 C\theta_2 \\ 0 & C\theta_1 & -S\theta_1 & -lS\theta_2 \\ -S\theta_2 & C\theta_2 S\theta_1 & C\theta_2 C\theta_1 & l+lC\theta_2 C\theta_1 \\ 0 & 0 & 0 & 1 \end{bmatrix},
\end{aligned} \tag{1}
$$

where $c\theta_1$means $\cos\theta_2$ and $s\theta_1$ means $\sin\theta_2$.

As shown by Figure 3, the vector closed quadrilateral (Wei *et al.*, 2018) $O_AA_1B_1O_B$ formed by the black solid line arrow can obtain the variation equation of the length A_iB_i of each wire-driven branch:

$$A_iB_i = O_AO_B + O_BB_i - O_AA_i (i = 1, 2, 3, 4). \tag{2}$$

In the equation, one end of the intermediate constraint branched chain U is connected to the fixed platform and the other end is connected to the mobile platform, so vector $O_BO_A = [\mathrm{l}\cdot S\theta_2 C\theta_1, -\mathrm{l}\cdot S\theta_1, \mathrm{l}+\mathrm{l}\cdot C\theta_2 C\theta_1]$. In the moving coordinate system O_B-$X_BY_BZ_B$, the coordinate of B_i can be expressed as $B_i = r(\cos\theta_i, \sin\theta_i, 0)^T$. In the static coordinate system O_A-$X_AY_AZ_A$, the coordinate of A_i can be expressed as $O_AA_i = A_i = r(\cos\theta_i, \sin\theta_i, 0)^T$ and $O_BB_i = {}^{A}_{B}RB_i$, $\theta_i = (2\pi/3)\times(i\text{-}1)$. By substituting O_BB_i and O_AA_i into Equation(2), the inverse solution of the driving branch chain vector length l_i position of the parallel trunk joint mechanism can be obtained as follows:

$$l_i = \left\| A_iB_i \right\| (i = 1, 2, 3, 4). \tag{3}$$

3.2 Velocity and acceleration models

The velocity Jacobian matrix of the trunk joint mechanism expresses the velocity relationship between the velocity of the flexible wire-driven branched chain and that of the moving platform. It can be obtained by Equation (3):

$$l_i = (O_AO_B + O_BB_i - O_AA_i)^T (O_AO_B + O_BB_i - O_AA_i), \tag{4}$$

Deriving the two ends of Equation (4) separately for time t can be obtained as follows:

$$l_i\dot{l}_i = (O_AO_B + O_BB_i - O_AA_i)^T\left(\dot{O_AO_B} + \dot{O_BB_i}\right). \tag{5}$$

In the equation, $\dot{O_AO_B} = V$ is the linear velocity of the mobile platform, $\dot{O_AB_i} = W \times O_BB_i$, w is the angular velocity of the mobile platform. Assuming $O_AO_B + O_BB_i - O_AA_i = q_i$, from Equation (5), we would know the following:

$$\dot{l}_i = q_i^T \cdot v + (O_BB_i \times q_i)^T \cdot \omega. \tag{6}$$

So, the velocity Jacobian matrix of the wire-driven 4-SPS/U rigid–flexible trunk joint mechanism can be expressed as follows:

$$J = \begin{bmatrix} p_1^T & (O_BB_1 \times p_1)^T \\ P_2^T & (O_BB_2 \times p_2)^T \\ P_3^T & (O_BB_3 \times p_3)^T \\ P_4^T & (O_BB_4 \times p_4)^T \end{bmatrix}. \tag{7}$$

As the mobile platform is connected by Hooke joint between the point at the center O_B and the constraint branched chain mechanism, so the linear velocity of the mobile platform is zero, that is $\dot{O_AO_B} = V = 0$. The result of substituting linear velocity V into Equation (6) is as follows:

$$\dot{l}_i = q_i^T \cdot \dot{O_BB_i} \cdot \omega. \tag{8}$$

In the equation, $\dot{O_AB_i} = \dot{{}^A_BR}B_i$ is the velocity of B_i. Let $J_i = q_i^T \cdot \dot{O_AB_i}$, the relationship between the velocity vectors $\dot{l}_i$ and $\dot{\omega}_i$ of each wire-driven branch is as follows:

$$\dot{l}_i = \begin{bmatrix} J_1 & J_2 & J_3 & J_4 \end{bmatrix}^T \cdot \begin{bmatrix} \dot{\theta}_1 & \dot{\theta}_2 \end{bmatrix}. \tag{9}$$

The acceleration equation of the wire-driven branch chain can be solved by taking the derivation of Equation (9) on both sides with respect to time t:

$$\ddot{l}_i = J\ddot{\omega} + \dot{J}\dot{\omega}. \tag{10}$$

In the equation, $\dot{J} = \begin{bmatrix} \dot{J}_1 & \dot{J}_2 & \dot{J}_3 & \dot{J}_4 \end{bmatrix}^T$ is the acceleration Jacobian matrix of wire-driven 4-SPS/U rigid–flexible trunk joint mechanism, which is expressed as follows:

$$\begin{cases} \dot{J}_1 = \frac{1}{l_1^2}\left(\dot{J}_{11} \cdot l_1 - J_{11} \cdot \dot{l}_1\right) \\ \dot{J}_2 = \frac{1}{l_2^2}\left(\dot{J}_{21} \cdot l_2 - J_{21} \cdot \dot{l}_2\right) \\ \dot{J}_3 = \frac{1}{l_3^2}\left(\dot{J}_{31} \cdot l_3 - J_{31} \cdot \dot{l}_3\right) \\ \dot{J}_4 = \frac{1}{l_4^2}\left(\dot{J}_{41} \cdot l_4 - J_{41} \cdot \dot{l}_4\right) \end{cases}. \tag{11}$$

4. Kinematic performance analysis of the wire-driven 4-SPS/U rigid–flexible parallel trunk joint mechanism based on spring

4.1 stiffness performance of parallel trunk joint mechanism

The stiffness of the wire-driven 4-SPS/U rigid–flexible parallel trunk joint mechanism mainly depends on the slight displacement of the moving platform caused by the external force of the rope and the stiffness function of the elastic spring elastic deformation. Therefore, this paper uses the stiffness superposition method to calculate the stiffness of the rigid–flexible parallel trunk joint mechanism. It can be assumed that the wire force vector of wire-driven branching chain is $f_i=[f_1, f_2, f_3, f_4]^T$, and that the force vector applied on the terminal moving platform is $F_i=[F_1, F_2, F_3, F_4]^T$. The virtual displacement generated by the wire of wire-driven branching chain and moving platform is, respectively, $\triangle S_i=[\triangle S_1, \triangle S_2, \triangle S_3, \triangle S_4]$ and $\triangle h_i=[\triangle h_1, \triangle h_2, \triangle h_3, \triangle h_4]$. Then, the virtual work (Gosselin, 1990) of the force vector on the wire end and actuator is expressed as follows:

$$f_i^T \Delta S_i = F_i^T \Delta h_i. \tag{12}$$

The input–output relationship between the velocity of each drive joint and the terminal execution velocity is $\triangle S_i=J\cdot\triangle h_i$. Assuming that the stiffness coefficient of each wire-driven branch chain is K_i, $f_i=k_i\cdot\triangle S_i$ can be obtained. By substituting the above formula into equation (12), the following can be obtained:

$$K_s = J^T k_i J. \tag{13}$$

In the equation, K_s is the stiffness Jacobian matrix of the mechanism. Each diagonal element in $k_i=\text{dig}\ (k_1, k_2, k_3, k_4)$ represents the stiffness of the ith wire.

Let $V=[v\ w]^T$ be the pose spiral vector of the moving platform, $l=[l_1, l_2, l_3, l_4]^T$ be the length vector of the wire-driven branching chain, $\delta=[\delta_x, \delta_y, \delta_z]^T$ represents the differential position vector along the coordinate axis direction, $n=[n_x, n_y, n_z]^T$ represents the differential attitude vector around the coordinate axis, then the differential pose vector can be expressed as $S=[\delta, n]^T$. Suppose the spring stiffness of the ith wire-driven branching chain is H_i, then $T_i=H_i*dl_i$, where T_i represents the spring tension on the wire-driven branch chain, and dl_i represents the spring deformation of the i th wire-driven branch chain.

With the combination of $dl_i=J*S$ and $T_i=H_i*dl_i$, $T_i=H_i*J*S$ can be obtained. Both sides of this equation are multiplied by J^T to get $J^T*T_i=J^T*H_i*J*S$. Let $F"=J^T*T_i$, then $F"=J^T*H_i*J*S$ is obtained further, and finally the stiffness matrix of the mechanism can be expressed as $M_t=J^T*H_i*J$. From the stiffness matrix expression, it can be seen that the stiffness is affected by the spring deformation configuration of the wire-driven branch chain. From the spring stiffness formula $H_i=(G*d^4/8*n*D^3)$, the stiffness matrix M_t of the spring in the wire-driven branch chain can be obtained as follows:

$$M_t = J^T diag\left(\frac{Gd_1^3}{8nD_1^3}\ \ \frac{Gd_2^3}{8nD_2^3}\ \ \frac{Gd_3^3}{8nD_3^3}\ \ \frac{Gd_4^3}{8nD_4^3}\right) J. \tag{14}$$

In the equation, G is the shear modulus of the spring; d is the wire diameter of the spring; n is the effective number of turns of the spring; D is the outside diameter of the spring.

From Equations (13) and (14), the stiffness K_t of the wire-driven 4-SPS/U rigid–flexible parallel trunk joint mechanism based on spring can be obtained as follows:

$$K_t = K_s + M_t. \tag{15}$$

4.2 Kinematic dexterity of parallel trunk joint mechanism

The dexterity of the mechanism expresses the movement ability of the mechanism along the specified direction under the orientation. The condition number of the Jacobian matrix can be used to evaluate the dexterity of the mechanism. Defined by the universal norm of the matrix (Li-jie, 2006):

$$\begin{cases} \|J\| = \sqrt{\alpha_{\max}\left(J^T J\right)} \\ \|J^{-1}\| = \frac{1}{\sqrt{\alpha_{\min}\left(J^T J\right)}} \end{cases}. \tag{16}$$

In the equation, $\alpha_{\max}(J^T J)$ and $\alpha_{\min}(J^T J)$, respectively, represent the maximum eigenvalue and the minimum eigenvalue of the matrix; $\beta_{\max} = ½(\alpha_{\max}(J^T J))$ and $\beta_{\min} = ½(\alpha_{\min}(J^T J))$, respectively, represent the maximum and minimum singular values of the Jacobian matrix.

Generally, the reciprocal of condition number is used as the judgment index of dexterity. Assuming $Q_k = (1/(\|J\|\|J^{-1}\|))$, substituting Equation (16) into expression Q_k gives dexterity:

$$Q_K = \frac{\sqrt{\alpha_{\min}\left(J^T J\right)}}{\sqrt{\alpha_{\max}\left(J^T J\right)}} = \frac{\beta_{\min}}{\beta_{\max}}. \tag{17}$$

According to Equation (17), Q_k is the reciprocal of the number of Jacobian matrix. Its value range is $0 \leqslant Q_k \leqslant 1$. The smaller the Q_k value, the worse will be the flexibility of the mechanism and the larger will be the motion deviation. At this time, the change of input joint velocity of the mechanism will have a greater impact on the change of output velocity. When $Q_k = 1$, the mechanism has the best flexibility and is called isotropic mechanism. However, since Q_K only represents the local dexterity of the mechanism, it cannot reflect the overall flexibility of the mechanism. In this paper, the following global dexterity coefficient (Wei-fang, 2016) is adopted to comprehensively evaluate the flexibility of the rigid–flexible parallel trunk joint mechanism:

$$C = \frac{1}{\left(\sqrt[3]{\left(\left(\frac{1}{Q_k}\right)^2 + \left(\frac{1}{\beta_{\min}}\right)^2 + \left(\frac{1}{M}\right)^2/3\right)}\right)}. \tag{18}$$

In the equation, the greater the C value, the higher will be the overall dexterity of the mechanism.

5. Application example and mechanism performance analysis

The spring-based wire-driven 4-SPS/U rigid–flexible parallel trunk joint mechanism parameters are set as follows: $r = 178.5$ mm, $n = 200$ mm, $l_{\min} = 222.3$ mm, $l_{\max} = 515$ mm, $\theta_{\text{Bimax}} = 90°$, $\theta_{\text{Aimax}} = 90°$, $-45° \leqslant \theta_i \leqslant 45°$. The stiffness of wire K_i is 2000N·m/rad. $D_i = g_i \cdot d_i (0 \leqslant g_i \leqslant +\infty)$ relation exists in the spring parameter, and G is 7.2×10^{10} N/m.

5.1 Simulation analysis of stiffness performance of the parallel trunk joint mechanism

From Equation (13), through MATLAB simulation, the maximum and minimum eigenvalue distributions of the stiffness Jacobian matrix of the parallel trunk joint mechanism only affected by the wire can be obtained. As shown in Figure 4, the branch chain driven by two adjacent ropes varies with θ_1 and θ_2, and it is symmetrically decreasing distribution in the four angular directions. The stiffness value near the middle is larger; the minimum stiffness

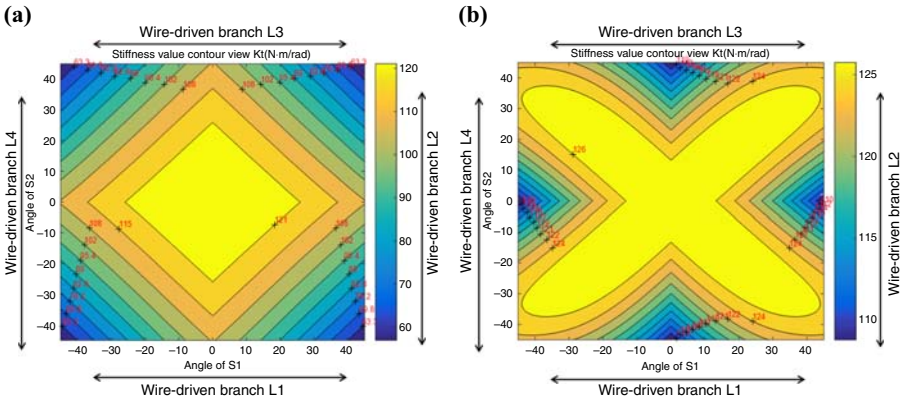

Notes: (a) Minimum eigenvalue distribution; (b) maximum eigenvalue distribution

Figure 4.
The eigenvalue distribution of stiffness matrix of the parallel trunk joint mechanism under the influence of wire only

in the direction of the minimum eigenvalue is 63 (N·m/rad), and the maximum stiffness in the direction of the maximum eigenvalue is 125 (N·m/rad). On this basis, a flexible spring is added to each wire-driven branch chain, and its elastic mechanism parameters are set as $d_i = 0.004$ m, $K_i = 6$, and $n_i = 4$ turns. From Equation (15), through MATLAB simulation, the stiffness matrix eigenvalue distribution of the parallel trunk joint mechanism can be obtained. As shown in Figure 5, the distribution variation of stiffness eigenvalues is the same as that in Figure 4. However, the minimum stiffness value in the direction of the minimum eigenvalue is 1,380 (N·m/rad), and the maximum stiffness value in the direction of the maximum eigenvalue is 2,750 (N·m/rad). Compared with the minimum maximum eigenvalue direction stiffness in Figure 4, which is only affected by the rope, the stiffness is increased by about 20 times. Therefore, adding a flexible spring to the wire-driven branch can improve the stiffness of the wire-driven 4SPS/U flexible rigid parallel joint mechanism.

According to Equation (14), the stiffness of the mechanism is affected by the spring elastic structure parameter ni, di, Di. In order to obtain the influence of degree of spring elastic structure parameters on the stiffness value of the mechanism, this paper obtained the maximum and minimum eigenvalue distributions of the Jacobian matrix of stiffness through the simulation based on Equation (15) under the condition of changing the

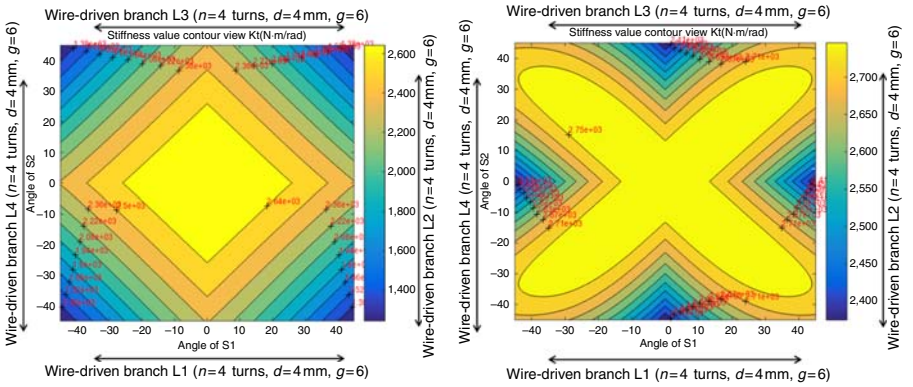

Notes: (a) Minimum eigenvalue distribution; (b) maximum eigenvalue distribution

Figure 5.
The eigenvalue distribution of stiffness matrix of the parallel trunk joint mechanism when the number of turns, wire diameter and outside diameter ratio of spring structure of each wire-driven branch chain are 4, 4 and 6 mm, respectively

parameters of spring elastic structure. Figure 6 shows the eigenvalue distribution of stiffness matrix of the parallel trunk joint mechanism when the number of turns in the spring structure of each wire-driven branching chain is 1, 2, 3, 4, and the wire diameter and outside diameter ratio are 4 mm, 6, respectively. Figure 7 shows the eigenvalue distribution of stiffness matrix of the parallel trunk joint mechanism when the linear diameter of the spring structure of each wire-driven branch chain is 10 mm, 20 mm, 30 mm and 4 mm, respectively, and the number of turns and outside diameter ratio are 4 and 6, respectively.

Figure 8 shows the eigenvalue distribution of stiffness matrix of the parallel trunk joint mechanism when the outer diameter ratio of the spring structure of each wire-driven branch is taken as 3, 4, 6, and 9, respectively, and the number of turns and the wire diameter are 4 and 4 mm, respectively. It can be seen from the distribution of the contour values of the stiffness values between the adjacent two wire-driven branches in each of the attached diagrams in Figures 6–8 in the shape of a ring that is different in size and sparse. When the spring elastic structure parameters on the adjacent two wire-driven branches take different values, the change in the stiffness values in the direction of the maximum and minimum characteristic values is: the distribution is reduced in different sizes in the direction of the four corners with the change

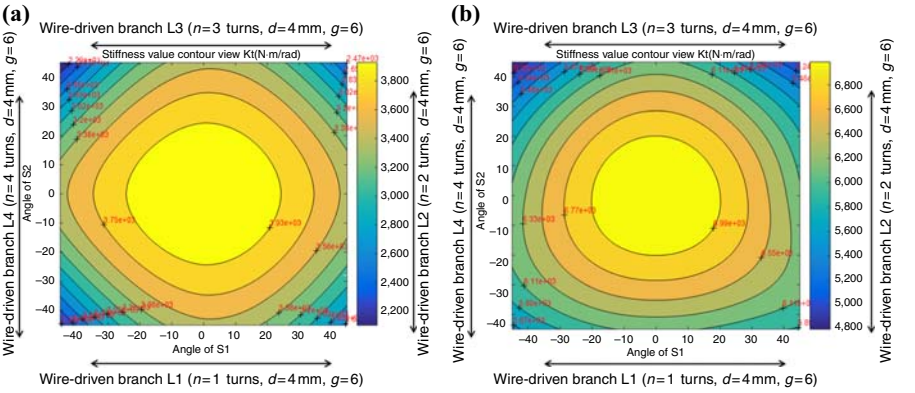

Figure 6.
The eigenvalue distribution of stiffness matrix of the parallel trunk joint mechanism when the number of turns in the spring structure of each wire-driven branching chain is 1, 2, 3, 4, and the wire diameter and outside diameter ratio are 4 and 6 mm, respectively

Notes: (a) Minimum eigenvalue distribution; (b) maximum eigenvalue distribution

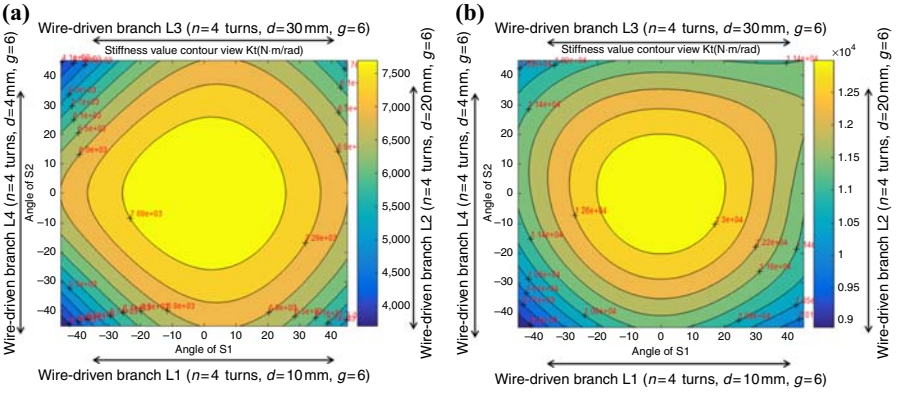

Figure 7.
The eigenvalue distribution of stiffness matrix of the parallel trunk joint mechanism when the linear diameter of the spring structure of each wire-driven branch chain is 10, 20, 30 and 4 mm, respectively, and the number of turns and outside diameter ratio are 4 and 6, respectively

Notes: (a) Minimum eigenvalue distribution; (b) maximum eigenvalue distribution

of θ_1 and θ_2 in the four angular directions – the closer to the middle, the greater will be the stiffness value. The smaller the number of the spring elastic structure turns of each adjacent two wire-driven branches in Figure 6, the greater will be the contour value of stiffness between the adjacent two wire-driven branch chains. The larger the linear diameter of the spring elastic structure of each adjacent two wire-driven branches in Figure 7, the greater will be the contour value of stiffnes between the adjacent two wire-driven branches. The smaller the outer diameter of the spring elastic structure of each adjacent two wire-driven branches in Figure 8, the larger will be the contour value of stiffness between the adjacent two rope-driven branches.

Therefore, by changing the spring elastic structural parameters of each wire-driven branch chain, the following can be concluded: the fewer the number of turns, the larger will be the wire diameter and the smaller will be the outer diameter. It can make the parallel trunk joint mechanism simplify and reduce the complexity of the structure, combined with the characteristics of wire-driven and rigid parallel mechanism that can effectively enhance and improve the parallel trunk joint mechanism of the specific direction of the maximum and minimum eigenvalue direction stiffness distribution. It ensures that the multi-motion mode hexapod mobile robot can meet the requirement of sufficient different stiffness for different motion postures through the parallel trunk joint mechanism.

As can be seen from the above description of Figures 4–8, it can only be explained that the spring elastic structure parameters have different influence on the stiffness value of the mechanism in the direction of the maximum and minimum eigenvalues, because the eigenvalues of stiffness along different eigenvectors are different, which cannot reflect that the elastic structural parameters of the spring have different absolute values of the stiffness values of the different pose positions of the mechanism. Therefore, we use the global stiffness K_p as the evaluation index. The larger the Kp, the better will be the global stiffness performance of the parallel trunk joint mechanism along the pose point. The global stiffness Kp is expressed as follows:

$$K_p = \sum_{i=1}^{S} \lambda_i(K_t). \tag{19}$$

In the equation, λ_i represents all the eigenvalues of the stiffness matrix K_t, and S represents the range of the workspace.

In order to obtain the influence degree of spring elastic structure parameters on the mechanism's global stiffness value, this paper obtained the global stiffness distribution through

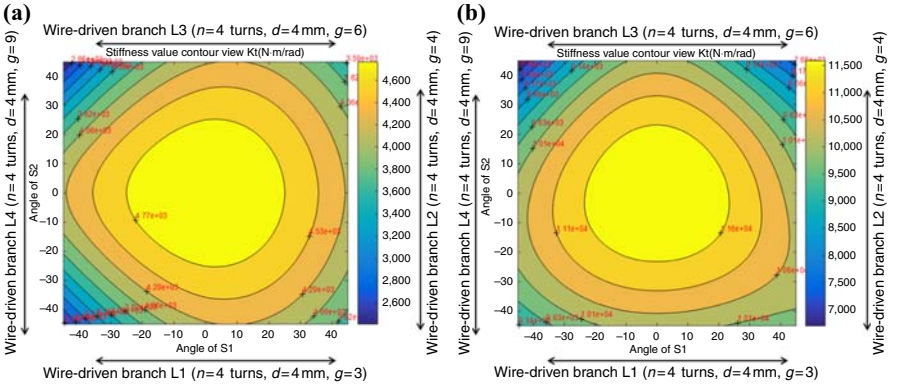

Notes: (a) Minimum eigenvalue distribution; (b) maximum eigenvalue distribution

Figure 8.
The eigenvalue distribution of stiffness matrix of the parallel trunk joint mechanism when the outer diameter ratio of the spring structure of each wire-driven branch is taken as 3, 4, 6, and 9, respectively, and the number of turns and the wire diameter are 4 and 4 mm, respectively

the simulation of Equation (19) by changing the spring elastic structure parameters. Figure 9 depicts the global stiffness distribution of the parallel trunk joint mechanism when the number of turns in the spring structure of each wire-driven branching chain is 1, 2, 3, 4, and wire diameter and outside diameter ratio are 4 mm and 6, respectively. Figure 10 depicts the global stiffness distribution of the parallel trunk joint mechanism when the linear diameter of the spring structure of each wire-driven branch chain is 10 mm, 20 mm, 30 mm and 4 mm, respectively, and the number of turns and outside diameter ratio are 4 and 6, respectively. Figure 11 depicts the global stiffness distribution of the parallel trunk joint mechanism when the outer diameter ratio of the spring structure of each wire-driven branch is taken as 2, 5, 8, and 9, respectively, and the number of turns and the wire diameter are 4 and 4 mm, respectively. According to Figures 9–11, the global stiffness value of the contour line between each adjacent two wire-driven branches is distributed in the form of rings with different sparse and sizes in the direction of the four corners. The stiffness value of the direction of the maximum and minimum eigenvalues is decreasing with the magnitude of θ_1 and θ_2 in the four angular directions – the closer to the middle, the greater will be the stiffness value. The smaller the number of the spring elastic structure turns of each adjacent two wire-driven branches in Figure 9, the larger will be the global stiffness value contour line value between the adjacent two wire-driven branches. The larger the linear diameter of the spring elastic structure of each adjacent two wire-driven branches in Figure 10, the larger will be the global stiffness value contour line value between the adjacent two wire-driven branches. The smaller the outer diameter of the spring elastic structure of each adjacent two wire-driven branches in Figure 11, the larger will be the global stiffness value contour line value between the adjacent two wire-driven branches.

Therefore, by changing the spring elastic structural parameters of each wire-driven branch chain, the following can be concluded: the fewer the number of turns, the larger will be the wire diameter and the smaller will be the outer diameter. It can effectively improve and adjust the

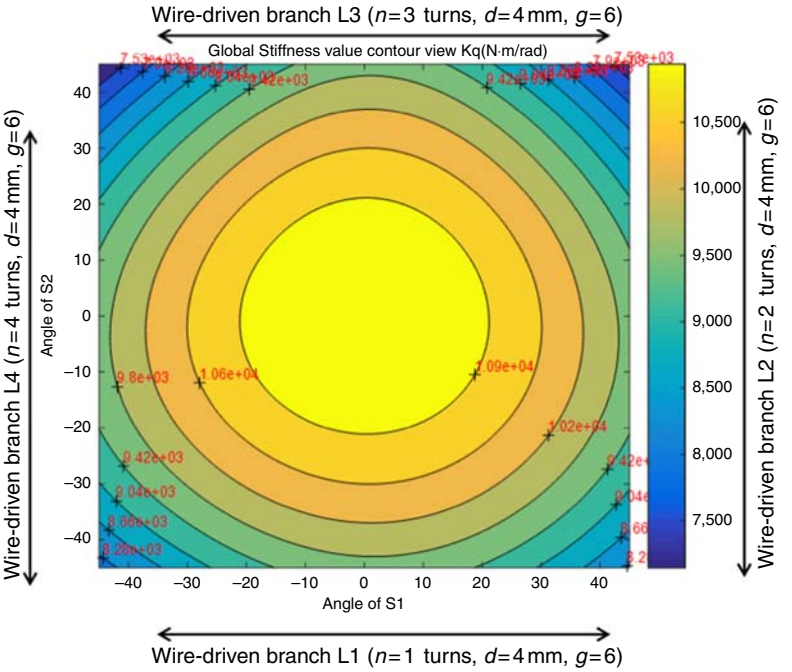

Figure 9.
Global stiffness distribution of the parallel trunk joint mechanism when the number of turns in the spring structure of each wire-driven branching chain is 1, 2, 3, 4, and the wire diameter and outside diameter ratio are 4 and 6 mm, respectively

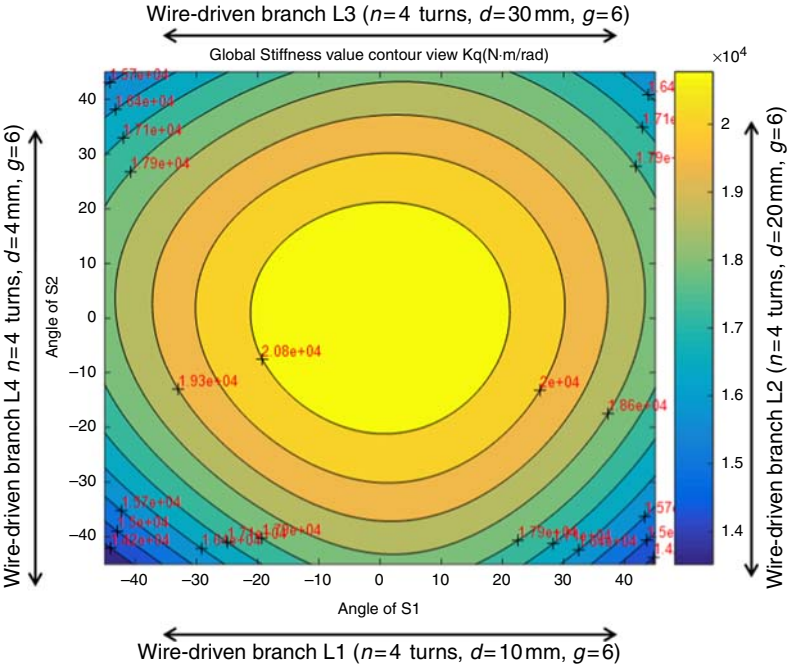

Figure 10.
Global stiffness distribution of the parallel trunk joint mechanism when the linear diameter of the spring structure of each wire-driven branch chain is 10, 20, 30 and 4 mm, respectively, and the number of turns and outside diameter ratio are 4 and 6, respectively

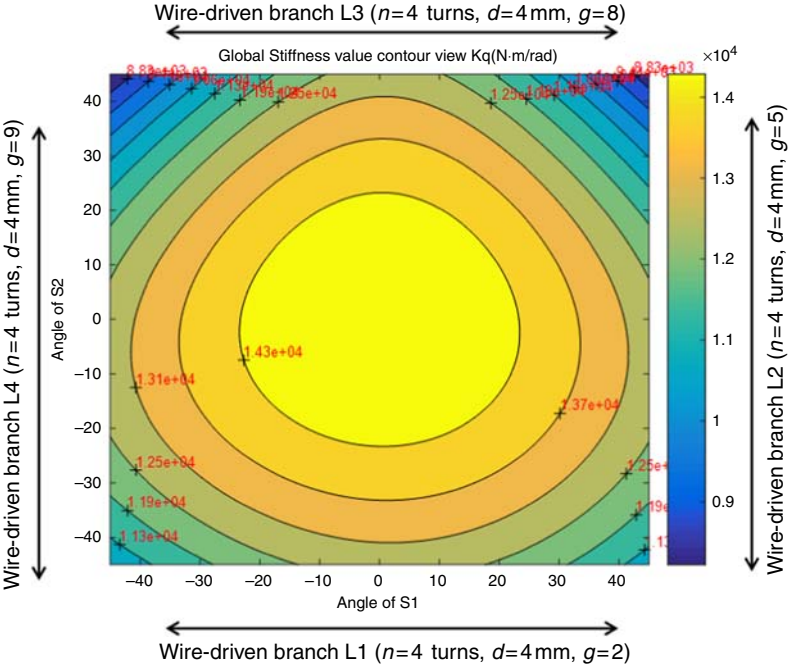

Figure 11.
Global stiffness distribution of the parallel trunk joint mechanism when the outer diameter ratio of the spring structure of each wire-driven branch is taken as 2, 5, 8, and 9, respectively, and the number of turns and the wire diameter are 4 and 4 mm, respectively

global stiffness and different distributions of the parallel trunk joint mechanism by combining the characteristics of wire-driven and rigid parallel mechanism after simplifying and reducing the structural complexity. It ensures that the multi-motion mode hexapod mobile robot in multi-motion mode can meet the performance requirement of global stiffness change at different pose points of different motion postures through the parallel trunk joint mechanism.

5.2 Analysis of motion dexterity

According to Equation (16), the singular minimum and maximum values of dexterity, as shown in Figures 12 and 13, can be obtained through MATLAB simulation. As can be seen from the figures, the singular maximum and minimum values of the dexterity of the parallel trunk joint mechanism have similar distribution rules, both of which are symmetric about the *Y*-axis and the *X*-axis, and have a maximum value of 252.43 near the center of the circle (0, 0). Their singular maximum and minimum values decrease along both sides of the symmetry axis, with a minimum value of 168.72 at the edge. It shows that the overall transmission performance and bearing capacity of the parallel trunk joint mechanism are better.

According to Equation (17), the local dexterity of the trunk joint mechanism shown in Figure 14 can be obtained by MATLAB simulation. It can be seen from the diagram that the maximum value of dexterity is 0.971 and the minimum value is 0.679, and the local dexterity is symmetrically distributed with *Y*-axis or *X*-axis as symmetry axis. At the same time, it can be seen that the closer to the symmetry axis, the greater will be the local dexterity, and the radiation decreases to both sides. The curved surface is smooth and continuous without peak mutation, which indicates that the parallel trunk joint mechanism has good local dexterity.

According to Equation (18), the global dexterity, as shown in Figure 15, can be obtained through MATLAB simulation. Compared with the local dexterity in Figure 14, the global dexterity has the same distribution law as the local dexterity, but the maximum global dexterity is 0.999 and the minimum is 0.77266, which is higher than that of the local dexterity. It shows that the global motion performance of the parallel trunk joint mechanism is more flexible and superior.

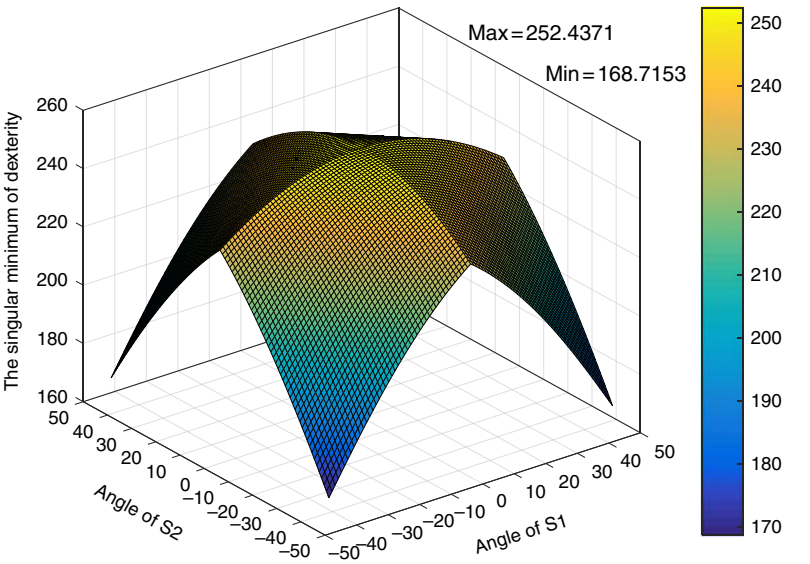

Figure 12.
Singular minimum distribution of dexterity

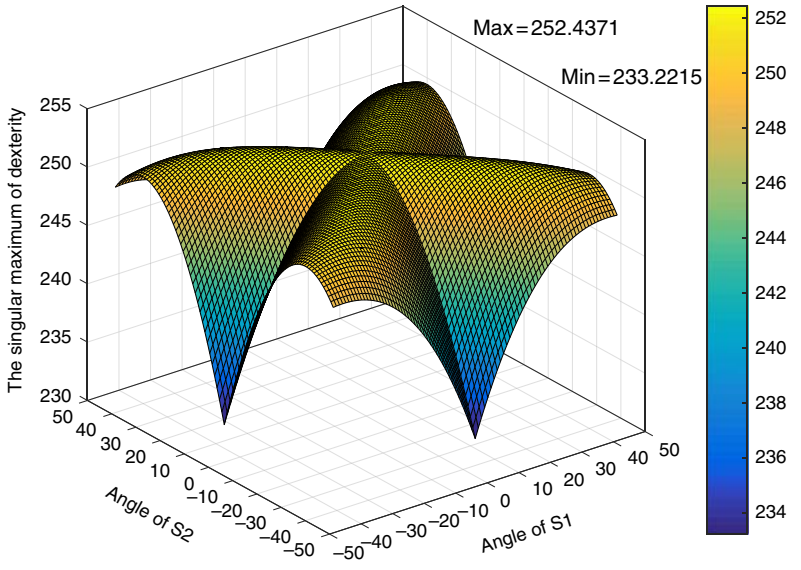

Figure 13.
Singular maximum distribution of dexterity

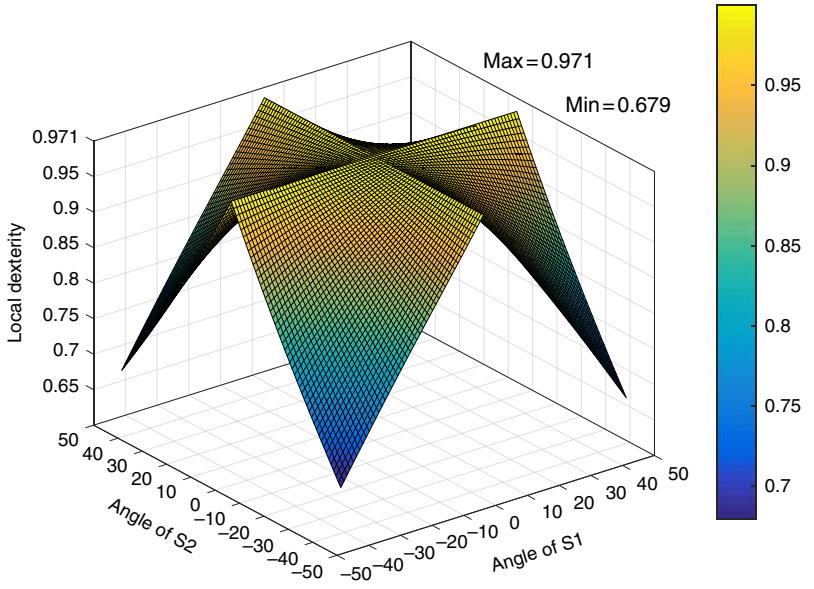

Figure 14.
Distribution of local dexterity

6. Conclusion

(1) Based on the spring-based wire-driven 4SPS/U rigid–flexible parallel trunk joint mechanism and using the closed vector method to establish the position inverse equation, the Jacobian matrix of velocity and acceleration is solved. On the basis of this and combined with the flexible deformation mechanism of the wire driven pair and the spring restrained pair, the stiffness matrix of the mechanism is derived.

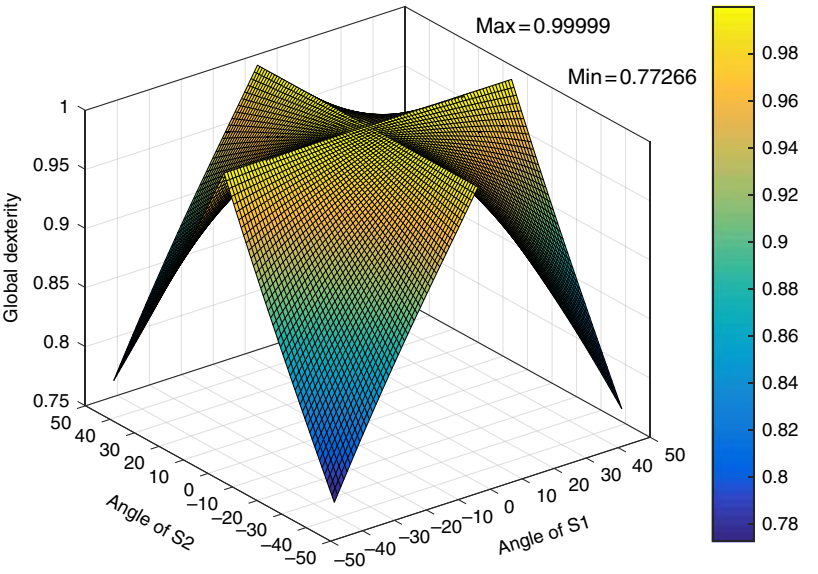

Figure 15.
Global dexterity distribution

(2) In this paper, the minimum and maximum eigenvalue distributions of stiffness matrix and the global stiffness index are taken as the stiffness evaluation indexes of the mechanism, and the simulation is carried out in the numerical software. The influence of the stiffness distribution on the parallel trunk joint mechanism after the introduction of the spring on the wire drive branch is compared and analyzed. It is concluded that by adjusting the spring elastic structural parameter variation, the stiffness of the mechanism in a specific direction can be improved, and the stiffness characteristic distribution of the original parallel mechanism can be improved to some extent.

(3) Finally, the dexterity of the mechanism is analyzed by numerical simulation map, in which the maximum and minimum values of the singularity of dexterity decrease with X or Y-axis symmetric decline, and the singular value difference from the workspace center to the boundary position is less. At the same time, the distribution maps of local dexterity and global dexterity are compared, and the results show that the parallel trunk joint mechanism has not only good bearing capacity and transmission performance, but it also has a more flexible movement performance.

References

Beira, R., Lopes, M., Praga, M., Santos-Victor, J., Bernardino, A., Metta, G. and Saltaren, R. (2006), "Design of the robot-cub (i Cub) head", *Proceedings – IEEE International Conference on Robotics and Automation. IEEE International Conference on Robotics and Biomimetics, Orlando, FL*, pp. 94-100.

Cong-hao, W., Chun, Z., Jia-yi, L. and Chun-tao, Z. (2018), "Design and simulation analysis of rope-driven bionic joints", *Mechanical Engineer*, No. 5, pp. 13-15.

Craig, J.J. (2009), *Introduction to Robotics: Mechanics and Control*, 3rd ed., Pearson Education India, pp. 1-164.

Dong-tao, X., Zhi-li, S. and Xiao-guang, D. (2013), "Stiffness characteristic analysis of modified Delta parallel mechanism based on bars' elastic deformation", *Transactions of the Chinese Society for Agricultural Machinery*, Vol. 44 No. 5, pp. 294-298.

Fan, L. (2014), "Analysis of cable-spring hybrid mechanism characteristics", Xidian University of Electronic Technology, Xian.

Gosselin, C. (1990), "Stiffness mapping for parallel ManiPulators", *IEEE Transactions on Robotics and Automation*, Vol. 6 No. 3, pp. 377-382.

Hai-wei, C., Jing-yuan, C., Xiang, C. and Yuan, J. (2013), "Stiffness analysis and optimization of a novel cable-driven anthropomorphic-arm manipulator", *Huazhong University of Science and Technology*, Vol. 41 No. 2, pp. 13-15.

Huang Hu-lin, A. (2016), "3-DOF Series-parallel Structure Torso Design in Humanoid Robots", Beijing Institute of Technology, Beijing.

Jian-feng, L., Shi-cai, L., Chun-jing, T., Run, J., Chenghui, X. and Zhaojing, Z. (2016), "Parallel 2-UPS/RRR ankle rehabilitation mechanism and kinematic performance analysis", *Robot*, Vol. 38 No. 2, pp. 145-153.

Jun, W. (2016), "Study on the variable stiffness cable driven study on the variable stiffness cable driven", University of Chinese Academy of Sciences, Beijing.

Kanehiro, F., Kaneko, K., Fujiwara, K., Harada, K., Kajita, S., Yokoi, K. and Isozumi, T. (2003), "The first humanoid robot that has the same size as a human and that can lie down and get up", *IEEE International Conference on Robotics & Automation. National Institute of Advanced Industrial Science and Technology, Tsukuba and Taipei*, pp. 1633-1639.

Li-jie, Z. (2006), "Performance analysis and dimension optimization of 2-Dof Parallel Manipulators", Yanshan University, Qinhuangdao.

Metta, G., Sandini, G., Vernon, D., Natale, L. and Nori, F. (2008), "The i Cub humanoid robot: an open platform for research in embodied cognition", *Proceedings of the 8th Workshop on Performance Metrics for Intelligent Systems. National Institute of Standards and Technology, ACM*, pp. 50-56.

Ogura, Y., Aikawa, H., Shimomura, K., Kondo, H., Morishima, A., Lim, H.O. and Takanishi, A. (2006), "Development of a new humanoid robot WABIAN-2", *Proceedings-IEEE International Conference on Robotics and Automation. National Institute of Advanced Industrial Science and Technology, Tsukuba and Taipei*, pp. 76-81.

Portman, V.T., Chapsky, V.S. and Shneor, Y. (2012), "Workspace of parallel kinematics machines with minimum stiffness limits: collinear stiffness value based approach", *Mechanism and Machine Theory*, No. 49, pp. 67-86.

Qing-huan, L., Qing-juan, D., Fan, L. and Xue-chao, D. (2017), "Stiffness analysis of a cable-driven parallel robot by adding springs", *Journal of Vibration and Shock*, Vol. 36 No. 10, pp. 198-223.

Qi-zhi, Y., Meng-tao, S., Xin-po, M., Jing, C. and Xingang, Z. (2018), "Design and analysis of rope driven joint for upper limb rehabilitation robot", *Journal of Jiangsu University*, Vol. 39 No. 5, pp. 563-569.

Run-tian, Y. (2016), "Design and analysis of a novel cable-driven parallel mechanism for ankle rehabilitation", Beijing Jiaotong University, Beijing.

Trevisani, A., Gallina, P. and Williams, L. II (2006), "Cable-direct-drive robot(CDDR) with passive SCARA support: theory and simulation", *Journal of Intelligent and Robot Systems*, Vol. 46 No. 1, pp. 73-94.

Von Zitzewitz, J., Fehlberg, L., Bruckmann, T. and Vallery, H. (2013), *Use of Passively Guided Deflection Units and Energy-Storing Elements to Increase the Application Range of Wire Robot, Cable-Driven Parallel Robot*, Springer, Berlin, pp. 165-184.

Wei, L., Zhi-guang, M., Shun-xin, Z., Jian-jun, Z. and Ziqi, Y. (2018), "Kinematics analysis on the series-parallel mechanism of a novel cable-driven elbow and wrist rehabilitation robot", *Journal of Journal of University of Technology*, Vol. 47 No. 4, pp. 7-9.

Wei-fang, W. (2016), "Research on redundantly restrained cable-driven parallel mechanism for simulating force", Tsinghua University, Beijing.

Zhe-dong, X., Yu-xuan, J., Qi, S. and Xin-Ji, G. (2018), "Analysis the working space and kinematics of the micro 3-PSP parallel mechanism", *Journal of Mechanical Strength*, Vol. 4 No. 40, pp. 915-922.

Corresponding author
Yuan Chen can be contacted at: cyzghysy@sdu.edu.cn